InAs/GaAs quantum dot laser epitaxially grown on on-axis (001) GaAsOI substrate

Research Article | Vol. 29, No. 23 / 8 Nov 2021 / Optics Express 38465
Optics EXPRESS

InAs/GaAs quantum dot laser epitaxially grown on on-axis (001) GaAsOI substrate

HAO LIANG,[1,2] TINGTING JIN,[1,2] CHAODAN CHI,[1,2] JIALIANG SUN,[1,2] XIAOLEI ZHANG,[1,2,3] TIANGUI YOU,[1] MIN ZHOU,[1] JIAJIE LIN,[4,6] AND SHUMIN WANG[1,5,7]

[1]*State Key Laboratory of Functional Materials for Informatics, Shanghai Institute of Microsystem and Information Technology, CAS, Shanghai 200050, China*
[2]*Center of Materials Science and Optoelectronics Engineering, University of Chinese Academy of Sciences, Beijing 100049, China*
[3]*School of Information Science & Technology, ShanghaiTech University, Shanghai 201210, China*
[4]*College of information science and engineering, Jiaxing university, Jiaxing, Zhejiang, 314001, China*
[5]*Chalmers University of Technology, Department of Microtechnology and Nanoscience, Gothenburg 41296, Sweden*
[6]*jjlin@mail.sim.ac.cn*
[7]*shumin@mail.sim.ac.cn*

Abstract: Quantum dot (QD) laser as a light source for silicon optical integration has attracted great research attention because of the strategic vision of optical interconnection. In this paper, the communication band InAs QD ridge waveguide lasers were fabricated on GaAs-on-insulator (GaAsOI) substrate by combining ion-slicing technique and molecular beam epitaxy (MBE) growth. On the foundation of optimizing surface treatment processes, the InAs/$In_{0.13}Ga_{0.87}As$/GaAs dot-in-well (DWELL) lasers monolithically grown on a GaAsOI substrate were realized under pulsed operation at 20 °C. The static device measurements reveal comparable performance in terms of threshold current density, slope efficiency and output power between the QD lasers on GaAsOI and GaAs substrates. This work shows great potential to fabricate highly integrated light source on Si for photonic integrated circuits.

1. Introduction

Photonic integrated circuits (PICs) are considered as a key technology to break Moore's law and achieve higher information transmission rate, lower energy consumption and higher levels of integration, compared with the traditional integrated circuits technology [1–4]. As the basis of PICs technology, preparation of high-performance light source on silicon is still a big challenge [5,6]. Although an all-Si laser has been realized via an active Si nanocrystals layer with a high spatial density and mono-dispersion developed by using hydrogen silsesquioxane, highly integrated all-Si laser is still limited by excitation mode (optical pump) and low output power [7]. III-V materials show excellent performance such as direct bandgap, broad wavelength tuning range, high electron mobility and photoelectric conversion efficiency. Fully integrating III-V laser on Si is a simpler and more feasible method to realize the Si-based light source with respect to the all-Si laser scheme [6,8]. Compared to flip-chip bonding, direct epitaxial growth has more advantages in reducing manufacturing cost and promoting reliability of devices [9,10]. The major difficulty of epitaxial III-V materials on Si is the generation of high density of crystal defects including threading dislocations (TDs), antiphase boundaries (APBs) and micro-cracks, caused by lattice and thermal mismatch [11,12]. These problems significantly degrade optical, thermal and electrical performances of devices [13–16]. InAs quantum dot (QD) laser has been emerged as a light source candidate due to its excellent tolerance for TDs and advantages in communication band, and satisfies the demands as Si-based light source [17,18].

#438678 https://doi.org/10.1364/OE.438678
Journal © 2021 Received 2 Aug 2021; revised 21 Sep 2021; accepted 27 Oct 2021; published 3 Nov 2021

Optics EXPRESS

Many innovative approaches to restrain crystal defects and improve material quality have been proposed using special substrates and buffer layers. Generally, offcut Si substrates are selected to reduce the generation of APBs at the interface of III-V buffer and Si [19]. Moreover, utilizing strained-layer superlattices (SLSs) as dislocation filter layers (DFLs) is effective and proven to prevent TDs from propagation, leading to a high-quality GaAs buffer on Si [17,20]. Based on this approach, high performance electrically pumped lasers using InGaAs/GaAs SLSs as DFLs on a 4° offcut Si substrate have been reported [21–23]. But offcut Si substrates are not fully compatible with the standard industrial process for CMOS using on-axis (001) Si. In recent years, specially processed V-shape grating Si structure was used to replace the offcut substrate [24–26]. According to this idea, Wei *et. al* employed a homo-epitaxially grown (111)-faceted silicon on insulator (SOI) hollow structure as III-V buffer and subsequent InAs/GaAs QD laser structure growth and achieved SOI-based QD ridge lasers, moving a step forward in laser sources on SOI platform for PICs [15]. However, the thick buffer layers of Group IV and III-V grown in molecular beam epitaxy (MBE) chamber will not only significantly increase the whole process cost, but also increase the risk of generation of micro-cracks due to the raised aggregate thickness [27,28].

Ion-slicing technique utilizes ion beam implantation to transfer high-quality films of III-V substrates onto SOI substrates with wafer bonding, which completely avoids the problems of lattice mismatch in the epitaxial process of seed layer [29–32]. This provides a new way to integrate light source onto the SOI platform. Up to now, high-quality III-V films on insulator have been reported by applying this method including InP, GaAs and InAs, but to our knowledge the related lasers have not been realized [33–35]. In this work, we fabricated high-quality GaAs films on SiO_2/Si substrates forming GaAsOI by ion-slicing technique. A clean and flat surface of the GaAsOI substrate was obtained after optimal surface treatment. Electrically pumped communication band InAs QD edge emitting laser directly grown on on-axis (001) GaAsOI substrates by MBE is demonstrated. Figure 1 shows the process flow chart of this technique.

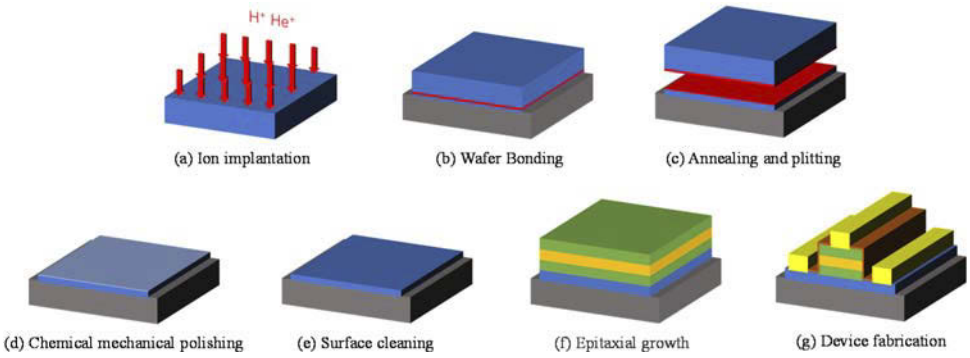

Fig. 1. Fabrication process of InAs QD laser on GaAsOI substrate.

2. Experiments

2.1. Surface treatment

In this work, three groups of (001) oriented semi-insulating GaAsOI substrates obtained by ion-slicing technique were prepared with different surface treatment processes named A, B and C before epitaxy, respectively, as shown in Table 1, where the symbol "√" indicates the process adopted. The initial preparations were adopted by removing the ion-damaged layer, chemical mechanical polishing (CMP), and surface chemical-cleaning procedures. The detailed surface treatment process is described as follows:

Optics EXPRESS

1. Removing the damaged layer: The GaAsOI wafers were immersed in a solution (20%HCl: 30%H_2O_2: H_2O = 1:1:30) at 25 °C for 25 s to completely etch away the ion-damaged GaAs layer. Next, the wafers were rinsed with deionized water (DI water) for 20 s.

2. Chemical mechanical polishing (CMP): CMP was used in order to reduce surface roughness. The wafers were polished with slurry of FuJimi company for 40 s and with DI water for 20 s at a high polishing speed (40 rpm), then rinsed with DI water for 10 s after polishing.

3. Acid-base cleaning: The wafers were first immersed in 98w% H_2SO_4 solution at 65 °C for 4 s and at 25 °C for 2 s successively. After being washed with DI water for 20 s, the GaAsOI wafers were quickly transferred into the 217 solutions (25%NH_4OH: 30%H_2O_2: H_2O = 2:1:7) at 25 °C for 5 s, then rinsed with DI water for 30 s.

4. Organic solvent cleaning: Acetone and ethanol were used for the ultrasonic cleaning for 10 minutes and repeated for 3 times, respectively. Finally, the wafers were cleaned with DI water for 5 minutes and dried with N_2.

Table 1. Surface treatment processes of sample A, B and C.

	Removing the damaged layer	CMP	Acid-base cleaning	Organic solvent cleaning
A	√			√
B		√		√
C		√	√	√

2.2. Buffer layer optimization

All epitaxial structures were grown on GaAsOI substrates using a DCA P600 solid-source MBE system. To ensure that the growth conditions of GaAs buffer layer on the three types of GaAsOI substrates are completely identical, all substrates were mounted side by side on the same 4-inch silicon substrate with melted indium. The GaAsOI substrates were outgassed at 350 °C for 1 hour in an ultra-high vacuum environment, and then heated to 580 °C measured by a pyrometer under the As_2 flux at a rate of 5 °C/min in order to avoid blistering and falling off of the GaAs thin template caused by high temperature during the heating process, and stayed for 5 minutes for deoxidation. A 1 μm GaAs buffer layer is grown on the substrates with a growth rate of 0.5 μm/h at 560 °C.

After optimizing surface of the GaAs buffer layer, a 1-layer InAs/$In_{0.13}Ga_{0.87}As$/GaAs dot-in-well (DWELL) structure and an uncapped InAs QDs structure, as shown in Fig. 2(a), were successively grown on a new batch of substrates. The test structure starts with a 600 nm GaAs buffer followed by a 200 nm GaAs/$Al_{0.4}Ga_{0.6}As$ superlattice (SL), 100 nm $Al_{0.4}Ga_{0.6}As$ cladding layer and 160 nm composition graded layer grown at 560 °C. Then 50 nm GaAs spacer layer and InAs QDs (2.5 ML) sandwiched by 2 nm and 6 nm $In_{0.13}Ga_{0.87}As$ were grown at 480 °C. The upper graded layer and cladding layer were grown in the same conditions as those for the lower part. Finally, a 50 nm GaAs layer and uncapped InAs QDs on 2 nm $In_{0.13}Ga_{0.87}As$ layer were sequentially deposited at 480 °C for morphology measurements.

2.3. Epitaxy of laser structure on GaAsOI

As shown in Fig. 2(b), a 3-layer InAs/$In_{0.13}Ga_{0.87}As$/GaAs DWELL laser structure was grown on the GaAsOI substrates pretreated by the method C. First, a 600 nm thick N-type GaAs bottom contact layer with a Si doping concentration of 4×10^{18} cm^{-3} was epitaxially grown on the GaAsOI substrate under the exact same conditions as above. Second, a ten-period $Al_{0.4}Ga_{0.6}As$/GaAs (10 nm/10 nm) SL was grown with the same doping level. The SL can

Optics EXPRESS

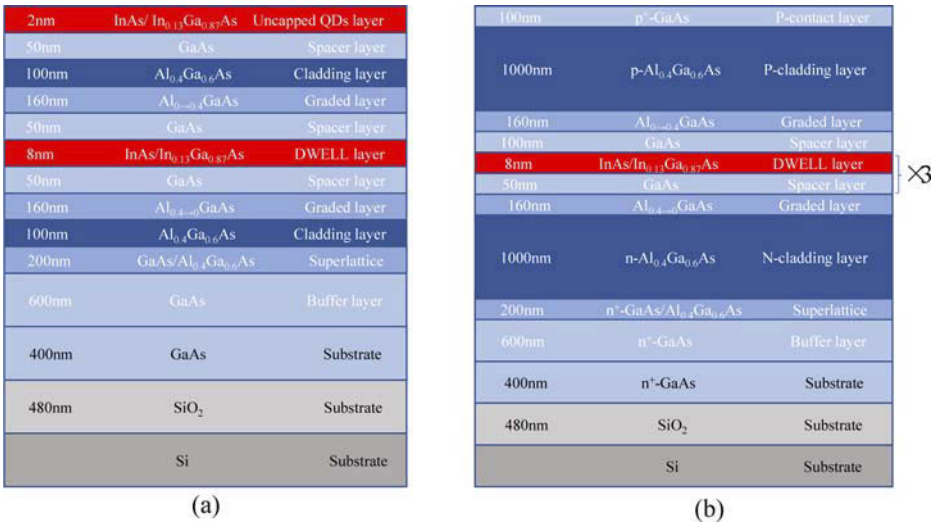

Fig. 2. (a) The test structure and (b) the laser structure grown on a GaAsOI substrate.

significantly improve quality of the active layers, thereby improving luminous efficiency of InAs QDs [36]. Then, a 1 μm thick $Al_{0.4}Ga_{0.6}As$ was grown as cladding layer, containing a 160 nm thick $Al_{0.4\rightarrow0}GaAs$ transition layer. Subsequently, a 3-layer InAs/$In_{0.13}Ga_{0.87}As$/GaAs DWELL laser active region, which consists of the InAs QDs (2.5 ML) sandwiched by 2 nm and 6 nm $In_{0.13}Ga_{0.87}As$, respectively, and separated by 50 nm GaAs spacer layers, was grown at 480 °C. Symmetrically, a 1 μm P-type $Al_{0.4}Ga_{0.6}As$ cladding layer was grown doped by Be. A 100 nm thick p^+ GaAs contact layer with a Be doping concentration of 2×10^{19} cm^{-3} completed the growth.

2.4. Fabrication of edge emitting lasers

Edge emitting lasers were fabricated with coplanar electrode contacts using a narrow-area Fabry-Perot (FP) cavity. Figure 3(a) shows the top view microphotograph of the InAs/$In_{0.13}Ga_{0.87}As$/GaAs DWELL laser device on a (001) GaAsOI substrate. The sawtooth passivated region as the vertical alignment mark of cavity facets separates the upper and lower electrodes. Laser strips with a 6-μm width were fabricated using standard optical lithography and wet etching techniques. Then Ti/Pt/Au (30nm/30nm/300nm) and Ge/Au/Ni/Au (13nm/33nm/30nm/200nm) were deposited on the p^+ GaAs contact layer and the exposed n^+ GaAs bottom contact layer to form metal electrodes using magnetron sputtering and electron beam evaporation technique, respectively. After lapping the backside Si to 100 μm, the structures were cleaved to make 5 mm long devices.

2.5. Material and device measurements

Optical microscope and atomic force microscope (AFM) were used to nondestructively assess surface morphology of the samples before and after epitaxial growth, including QD density, surface defects and roughness. High-resolution X-ray diffractometer (HRXRD) is used to characterize the overall quality of the epitaxial films. The optical properties of materials were measured in photoluminescence (PL) and lasing spectrum. Scanning electron microscopy (SEM) provided more detailed structural information. Cross-sectional bright-field transmission electron microscopy (TEM) was employed to reveal interface quality and structural defects such as dislocations after the sample was prepared by focused ion beam (FIB). Static characterizations of

Optics EXPRESS

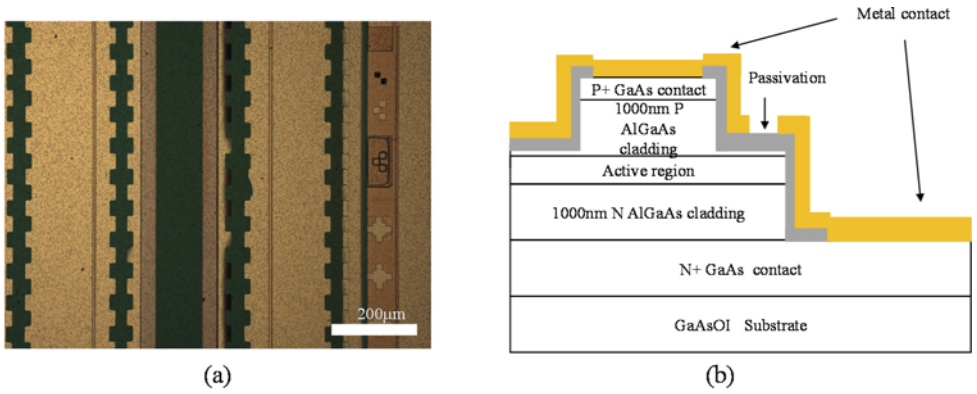

Fig. 3. (a) The microphotograph and (b) the schematic diagram of the laser devices on GaAsOI substrate.

the InAs/$In_{0.13}Ga_{0.87}As$/GaAs DWELL edge emitting laser devices were measured under pulsed current injection (a pulse frequency of 2 KHz and 20% duty cycle) at room temperature.

3. Results and discussions

3.1. Surface optimization and structural quality

The black line in Fig. 4(a) shows the HRXRD rocking curve of the virgin GaAsOI substrate without thermal post-annealing. A secondary peak on the left side of the main peak is observed due to the compressive strain caused by the residual ions (H^+ and He^+) in the lattice gap [37]. After a high temperature annealing at 400 °C for 1 hour, the residual ions and vacancy defects are redistributed due to thermal diffusion, and the secondary peak merges with the main peak shown by the red line. The full width at half maximum (FWHM) of the main peak is thus broadened from 86.9 arcsec to 139 arcsec. In Fig. 4(b), the root mean square value of surface roughness (R_q) as high as 14.6 nm of the virgin GaAsOI substrate is too high for further epitaxial growth. After being annealed at 400 °C for 1 hour, the R_q increases slightly to 17.0 nm, as shown in Fig. 4(c). The surface morphology has no obvious change before and after the annealing.

A series of surface treatment processes are used to improve the surface quality of the virgin GaAsOI substrates. Three groups of samples were obtained as shown in Table 1. Surface morphology of sample A and B is shown in Fig. 5, obtained by optical microscope, AFM and SEM, respectively. Sample A reveals severe dust pollution (shown in Fig. 5(a)) and pit defects

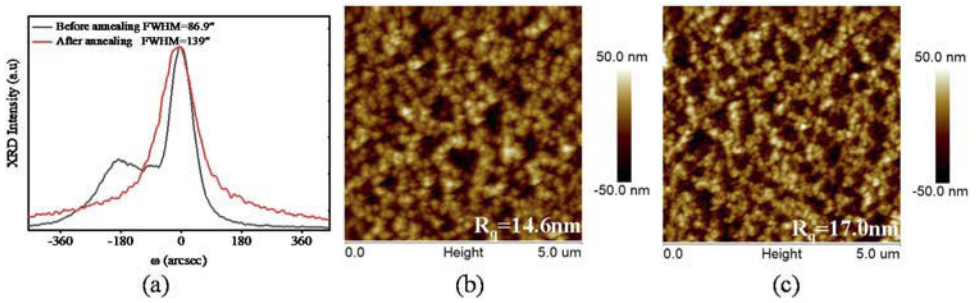

Fig. 4. (a) HRXRD rocking curves of the GaAsOI before and after the annealing. (b) Before and (c) after the annealing, 5×5 μm^2 AFM images of the GaAsOI substrate.

Optics EXPRESS

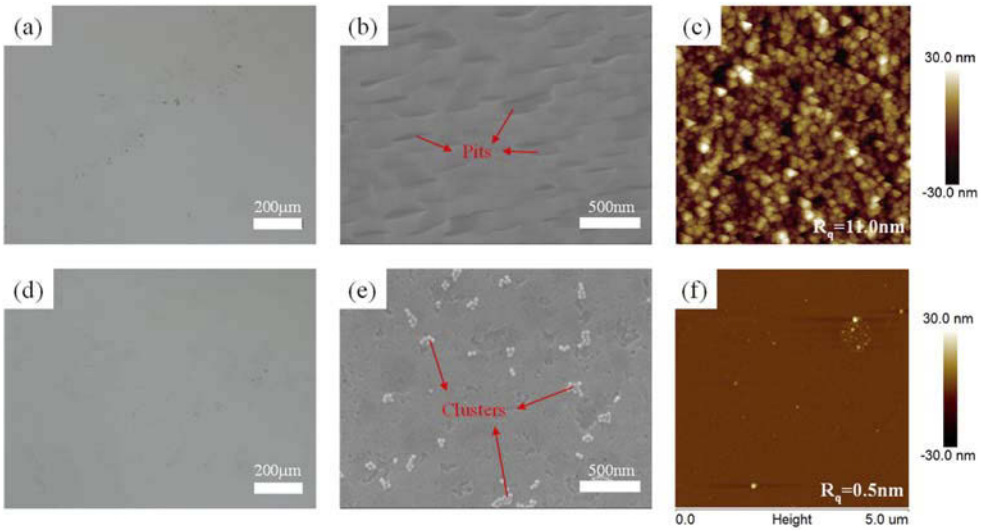

Fig. 5. Surface#morphology of (a, b, c) sample A and (d, e, f) sample B obtained by optical microscope, SEM and AFM, respectively.

(shown in Fig. 5(b)) on surface after removal of the ion damaged layer and organic cleaning, and its R_q (shown in Fig. 5(c)) is as high as 11.0 nm in a 5×5 μm^2 area. These pit defects are mostly rectangular in shape with a length below 500 nm and a width above 10 nm. Although wet etching can remove the surface damage layer, the improvement of surface roughness is not visible. Wet etching is replaced by CMP in sample B, AFM image of sample B shows that the R_q (shown in Fig. 5(f)) has been significantly decreased to 0.5 nm in a 5×5 μm^2 area. But the particle pollution on the surface shown in photomicrograph (Fig. 5(d)) still exists. Nanoparticle clusters on the surface can be clearly observed by SEM in Fig. 5(e).

In order to explore the source of these nanoparticles that are difficult to be removed by organic cleaning, we estimate that the diameter of the nanoparticles is about 25-30 nm and the density is about 2.72×10^7 cm^{-2} from the SEM image of Fig. 6(a). These nanoparticles show an irregularly aggregated morphology. Based on the extremely consistent particle size, we suspect that the nanoparticles come from the abrasive particles of the polishing slurry. In addition, the energy dispersive spectroscopy (EDS) surface scanning was selected to analyze element composition of the region. As shown in Fig. 6(b), there is no relationship between the nanoparticles and main elements like Si and C of abrasive particles. So, nanoparticles still could come from debris produced by CMP.

From the above results of elemental analysis of nanoparticles and combined with previous research results of GaAs surface cleaning [38,39], sample C adds an acid-base cleaning process based on the process B. From both optical microscopy and SEM images in Fig. 7(a) and (b), the surface nanoparticles are entirely removed. The AFM image in Fig. 7(c) also shows a better surface quality and outstanding surface roughness of 0.7 nm without nanoparticles. However, a few pits (the dark areas shown in Fig. 7(c)) like that on sample A can still be observed on the surface of sample C, but their size and depth are significantly reduced.

A 1 μm thick GaAs buffer layer was epitaxially grown on the three groups of GaAsOI substrates. Surface morphology after growth is obtained by optical microscopy, SEM and AFM, respectively. As shown in Fig. 8(a), the optical microscopy shows many defects on the surface, which is likely due to dust pollution and large surface pit defects that destroy the integrity of extension surface. However, the R_q of sample A in Fig. 8(c) decreases from 11.0 nm to 7.32 nm after epitaxial

Optics EXPRESS

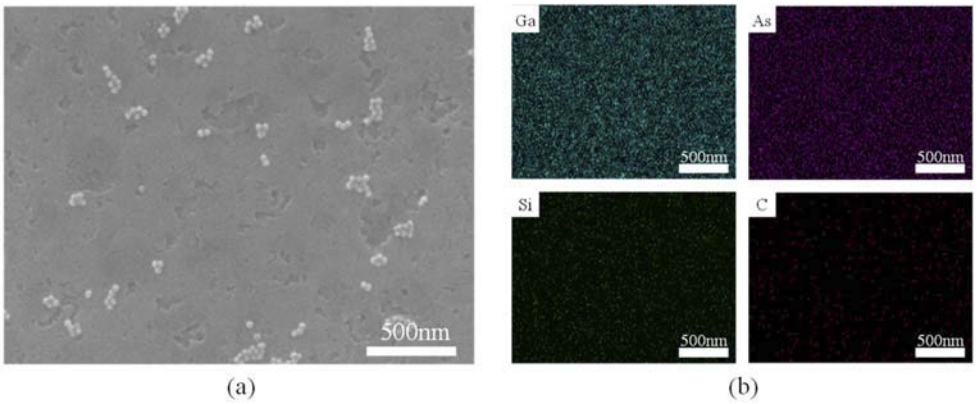

Fig. 6. (a) SEM image of nanoparticles on surface of sample B. (b) EDS images of elemental Ga, As, Si and C.

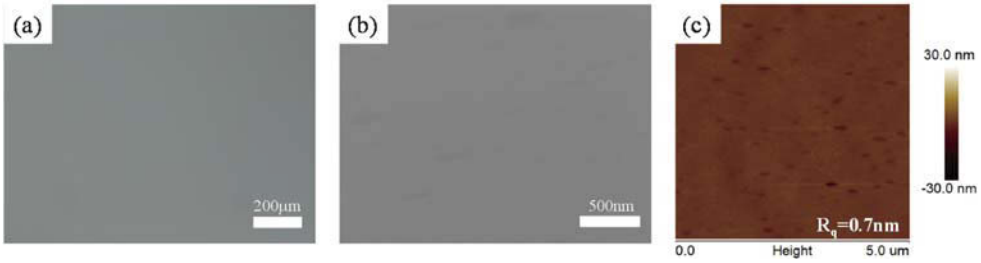

Fig. 7. Surface#morphology of sample C obtained by (a) optical microscopy, (b) SEM, and (c) AFM, respectively.

growth, which proves that the surface quality of GaAsOI can be improved using a homo-buffer. Although the surface roughness of sample B is as low as 0.5 nm, a large number of nanoparticles remain on the surface, which becomes the source of defects in the epitaxial process. Inferred from the results in Fig. 8(f), the negative effect of these nanoparticles on epitaxial growth is very severe, resulting in a high R_q value of 10.1 nm after 1 μm GaAs buffer. By eliminating nanoparticles in sample C, a smooth surface and low defect density of GaAs buffer (shown in Fig. 8(g)) with R_q value of 1.5 nm was obtained for subsequent device growth. The defects change from irregular shape to regular rhombic, and finally appear only in the strain bulge region. The defect density (1.3×10^4 cm^{-2} for sample A) can be reduced below 10^2 cm^{-2} for sample C. The maximum size of the defects is about 2 μm. According to Wang *et. al*, these defects come mainly from substrate contamination [40].

In addition, HRXRD rocking curves of sample A, B and C before and after growth also show the change of the lattice quality of the epitaxial layer in Fig. 9. Due to the effects of high temperature annealing and defects, the FWHM was broadened significantly after growth. It was also observed that the FWHM of sample C (from 95.8 arcsec to 228.3 arcsec) was improved compared to the sample A (from 93.6 arcsec to 258.7 arcsec) and B (from 83.6 arcsec to 254.9 arcsec) after growth.

In order to characterize the optical quality of materials, a 1-layer InAs/$In_{0.13}Ga_{0.87}As$/GaAs DWELL structure and an uncapped InAs QDs structure, as shown in Fig. 2(a), were successively grown on a new batch of sample B, C and commercial GaAs substrate. The morphology of these uncapped QDs on sample C is shown in Fig. 10(a) with a density of 2.9×10^{10} cm^{-2}. Comparing Fig. 10(a) and (b), InAs QDs on sample C have a larger size caused by the slightly higher surface

Optics EXPRESS

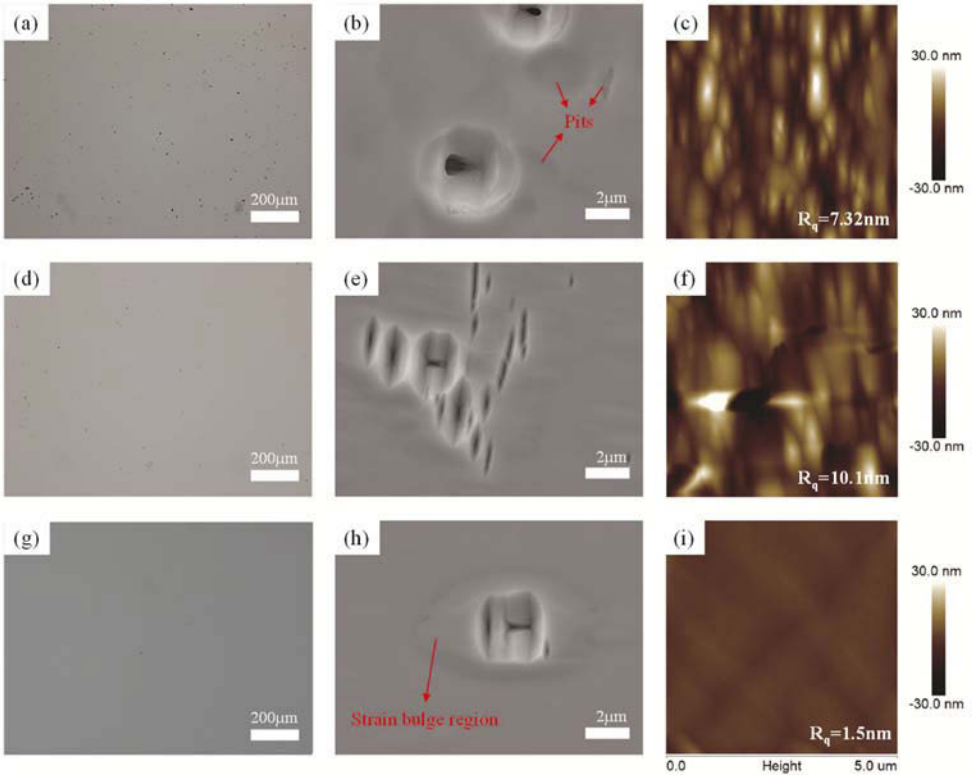

Fig. 8. Surface morphology of (a, b, c) sample A, (d, e, f) sample B and (g, h, i) sample C after growth of 1 mm thick GaAs buffer obtained by optical microscopy, SEM and AFM, respectively.

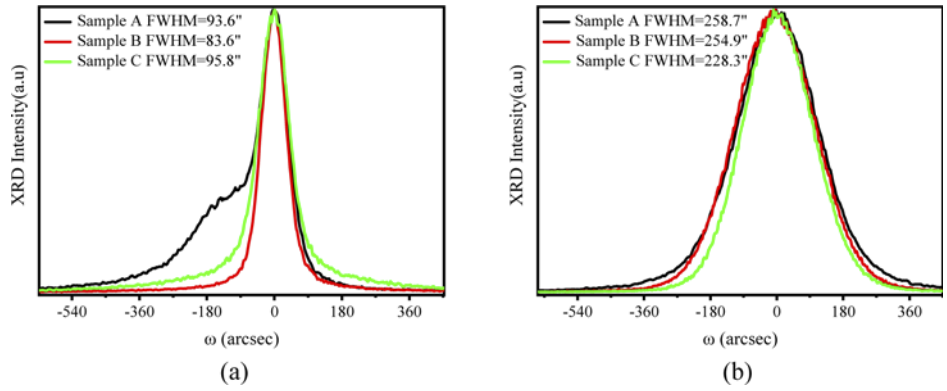

Fig. 9. HRXRD of sample A, B and C (a) before and (b) after growth.

temperature of Si substrate during the growth. From room temperature PL spectra in Fig. 10(c), the optical quality of sample C is also significantly improved compared with B and its intensity is about 72% of that of the GaAs substrate.

Optics EXPRESS

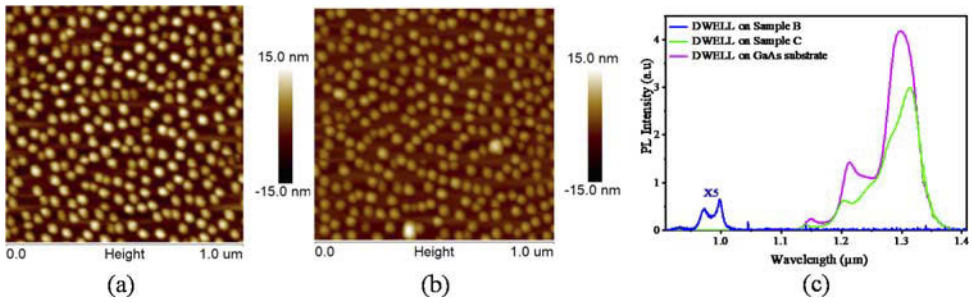

Fig. 10. AFM image of the uncapped InAs QDs on (a) sample C and (b) commercial GaAs substrate. (c) PL comparison of DWELL structures grown on sample B, C and GaAs substrates.

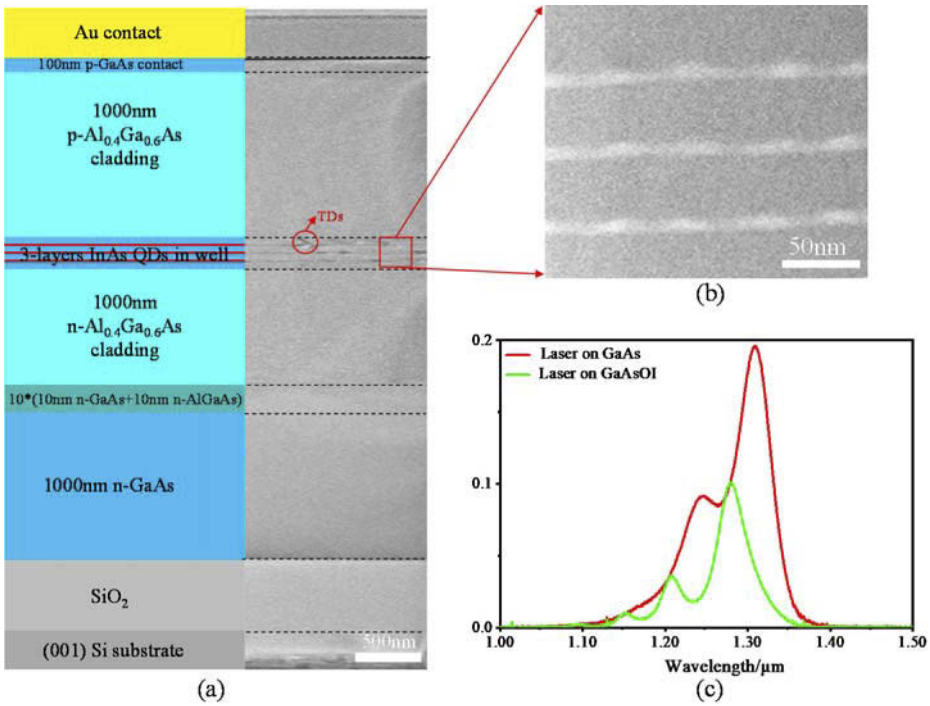

Fig. 11. (a) Cross sectional TEM image of the laser structure on GaAsOI substrate. (b) High resolution TEM image of InAs QDs. (c) PL comparison of laser structures grown on GaAsOI and GaAs substrates

3.2. *Laser performance*

Figure 11(a) illustrates a cross-sectional TEM image of the 3-layer InAs/$In_{0.13}Ga_{0.87}As$/GaAs DWELL laser structure, exhibiting high lattice quality of the defect-free epitaxial GaAs buffer layer growth on GaAsOI. The bonding interface between GaAs and SiO_2 can be clearly observed, which proves that the thermal mismatch between III-V layers and SiO_2 does not result in the debonding of interface during the epitaxial growth. A few dislocations appear from position near the third layer of QDs, which limits the number of QD layers to be 3 layers. A QD density of ~ 4.0 $\times 10^{10}$ cm^{-2} is estimated from the TEM image shown in Fig. 11(b), and the distribution of QDs shows an obvious vertically stacking phenomenon. Room temperature PL in Fig. 11(c) exhibits

Optics EXPRESS

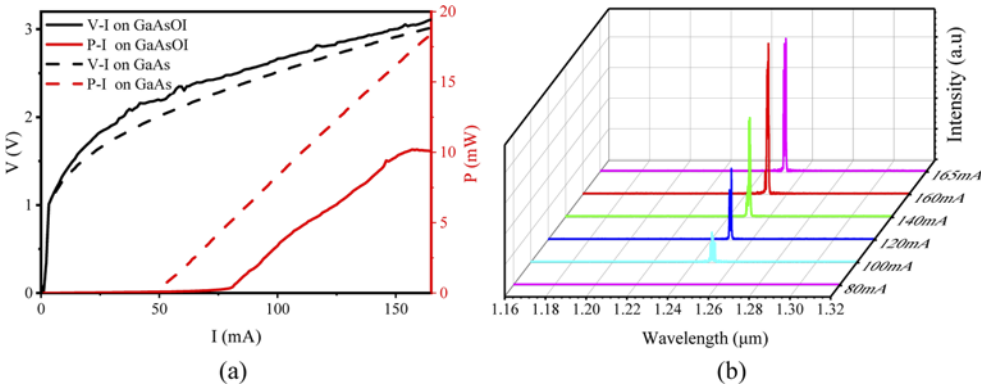

Fig. 12. (a) V-P-I curves of the InAs QD laser grown on GaAs and GaAsOI substrates under pulsed operation conditions at room temperature. (b) Emission spectra of the InAs QD laser on GaAsOI (001) substrate at various Injection currents.

emission peak wavelength at ~1280 nm with a FWHM of 35.4 meV. Due to the higher thermal conductivity of Si (150 W/mK) compared with GaAs (46 W/mK), the actual growth temperature of GaAsOI is slightly higher than that of the GaAs substrate. Therefore, the annealing effect of the capped InAs QDs during the epi-growth of the upper AlGaAs waveguide layer causes the PL center wavelength blue shift compared with the that on GaAs substrate.

Figure 12(a) shows the voltage and light output power-vs-current (V-P-I) curves of the InAs/$In_{0.13}Ga_{0.87}As$/GaAs DWELL laser grown on GaAsOI and GaAs substrates, respectively, under pulsed operation at 20 °C. The frequency of the pulse source is 2 KHz and the duty cycle is 20%. For the laser on GaAsOI, when the injection current is below 80 mA, only spontaneous emission is observed. By continuing to increase the current, the spontaneous emission is rapidly converted into multi-mode laser emission with a peak wavelength of 1250 nm in Fig. 12(b). The threshold current density is about 266.7 A/cm^2, corresponding to 88.9 A/cm^2 per QD layer. A single facet maximum output power is ~10.2 mW when the injection current reaches 160 mA. On the same test conditions, a low threshold current density of 55.6 A/cm^2 per QD layer and a high single facet maximum output power of 32 mW at 300 mA are obtained from the laser on GaAs substrates. The calculated slope efficiency and external differential quantum efficiency is ~0.12 W/A and 12%, respectively, which is close to 0.14 W/A and 14% on GaAs. By comparing the V-I curves, it can be found that the applied voltage of the laser on GaAsOI is slightly higher than that of the GaAs substrate at the same injection current, which indicates that the laser on GaAsOI has a larger series resistance due to the limited thickness of the bottom electrode. The large series resistance is caused by the lateral electron transport in the 1 μm thick n^+ GaAs contact layer and results in considerable Joule heat generation. The huge thermal effect also prevents the laser on GaAsOI from CW lasing, a focus for future improvement of the device performance.

4. Conclusion

In conclusion, we have successfully demonstrated the first communication band InAs/$In_{0.13}Ga_{0.87}As$/GaAs DWELL lasers on GaAsOI substrate by combining ion-slicing technique and MBE epitaxy. The lattice mismatch problem as Achilles' heel of traditional heteroepitaxial methods can be completely solved by using the novel GaAsOI substrates. Through a series of careful surface treatment including CMP and surface chemical-cleaning procedures, the density of surface defects is significantly reduced to be below 10^2 cm^{-2}. The Fabry–Perot narrow ridge lasers on GaAsOI substrate reveal a threshold current density of 88.9 A/cm^2 per QD layer and a high slope efficiency of 0.12 mW/A under pulsed operation at 20°C, comparable to those

Optics EXPRESS

from the similar QD lasers grown on GaAs substrates. Our work demonstrates a new way to realize communication band laser sources on GaAsOI substrate which is compatible with the existing CMOS platform technology. Meanwhile, it also provides a new method to integrate other optoelectrical devices on GaAsOI, such as photodetectors and VCSELs etc.

Funding. Key Technologies Research and Development Program (2017YFE0131300); National Natural Science Foundation of China (11622545, 11705262, 61804157, 61851406, 61874128, 61875220, U1732268); Key Research Program of Frontier Science, Chinese Academy of Sciences (QYZDY-SSWJSC032, ZDBS-LY-JSC009); Chinese-Austrian Cooperative Research and Development Project (GJHZ201950); Shanghai Science and Technology Innovation Action Plan Program (17511106202); Program of Shanghai Academic Research Leader (19XD1404600); Shanghai Youth Top Talent Program, Shanghai Sailing Program (19YF1456200, 19YF1456400); K. C. Wong Education Foundation (GJTD-2019-11); NCBiR within the Polish-China (WPC/130/NIR-Si/2018).

Disclosures. The authors declare no conflicts of interest related to this article.

Data availability. Data underlying the results presented in this paper are not publicly available at this time but may be obtained from the authors upon reasonable request.

References

1. D. A. B. Miller, "Device Requirements for Optical Interconnects to Silicon Chips," Proc. IEEE **97**(7), 1166–1185 (2009).
2. D. Thomson, A. Zilkie, J. E. Bowers, T. Komljenovic, G. T. Reed, L. Vivien, D. Marris-Morini, E. Cassan, L. Virot, J. M. Fedeli, J. M. Hartmann, J. H. Schmid, D. X. Xu, F. Boeuf, P. O'Brien, G. Z. Mashanovich, and M. Nedeljkovic, "Roadmap on silicon photonics," J. Opt. **18**(7), 073003 (2016).
3. X. Wang and J. Liu, "Emerging technologies in Si active photonics," J. Semicond. **39**(6), 061001 (2018).
4. Z. P. Zhou, R. X. Chen, X. B. Li, and T. T. Li, "Development trends in silicon photonics for data centers," Opt. Fiber Technol. **44**, 13–23 (2018).
5. D. Liang and J. E. Bowers, "Recent progress in lasers on silicon," Nat. Photonics **4**(8), 511–517 (2010).
6. S. Pan, V. Cao, M. Liao, Y. Lu, Z. Liu, M. Tang, S. Chen, A. Seeds, and H. Liu, "Recent progress in epitaxial growth of III-V quantum-dot lasers on silicon substrate," J. Semicond. **40**(10), 101302 (2019).
7. D. C. Wang, C. Zhang, P. Zeng, W. J. Zhou, L. Maa, H. T. Wang, Z. Q. Zhou, F. Hu, S. Y. Zhang, M. Lu, and X. Wu, "An all-silicon laser based on silicon nanocrystals with high optical gains," Sci. Bull. **63**(2), 75–77 (2018).
8. D. L. Huffaker, G. Park, Z. Zou, O. B. Shchekin, and D. G. Deppe, "1.3 mu m room-temperature GaAs-based quantum-dot laser," Appl. Phys. Lett. **73**(18), 2564–2566 (1998).
9. K. Tanabe, D. Guimard, D. Bordel, S. Iwamoto, and Y. Arakawa, "Electrically pumped 1.3 mu m room-temperature InAs/GaAs quantum dot lasers on Si substrates by metal-mediated wafer bonding and layer transfer," Opt. Express **18**(10), 10604–10608 (2010).
10. K. Tanabe, K. Watanabe, and Y. Arakawa, "III-V/Si hybrid photonic devices by direct fusion bonding," Sci. Rep. **2**(1), 349 (2012).
11. H. Uchida, M. Adachi, T. Egawa, H. Nishikawa, T. Jimbo, and M. Umeno, "High quality GaAs on Si grown by CBE," *Icds-18 - Proceedings of the 18th International Conference on Defects in Semiconductors*, Pts 1-4 196, 535–538 (1995).
12. K. Maehashi, H. Nakashima, F. Bertram, P. Veit, and J. Christen, "Molecular beam epitaxial growth and characterization of GaAs films on thin Si substrates," Jpn. J. Appl. Phys. **37**(Part 1, No. 1), 39–44 (1998).
13. A. D. Lee, Q. Jiang, M. C. Tang, Y. Y. Zhang, A. J. Seeds, and H. Y. Liu, "InAs/GaAs Quantum-Dot Lasers Monolithically Grown on Si, Ge, and Ge-on-Si Substrates," IEEE J. Sel. Top. Quantum Electron. **19**(4), 1901107 (2013).
14. J. Kwoen, B. Jang, K. Watanabe, and Y. Arakawa, "High-temperature continuous-wave operation of directly grown InAs/GaAs quantum dot lasers on on-axis Si (001)," Opt. Express **27**(3), 2681–2688 (2019).
15. W. Q. Wei, Q. Feng, J. J. Guo, M. C. Guo, J. H. Wang, Z. H. Wang, T. Wang, and J. J. Zhang, "InAs/GaAs quantum dot narrow ridge lasers epitaxially grown on SOI substrates for silicon photonic integration," Opt. Express **28**(18), 26555–26563 (2020).
16. M. C. Tang, J. Wu, S. M. Chen, Q. Jiang, A. J. Seeds, H. Y. Liu, V. G. Dorogan, M. Benamara, Y. Mazur, and G. Salamo, "Optimisation of the dislocation filter layers in 1.3-mu m InAs/GaAs quantum-dot lasers monolithically grown on Si substrates," IET Optoelectron. **9**(2), 61–64 (2015).
17. J. Wu, A. Lee, Q. Jiang, M. C. Tang, A. J. Seeds, and H. Y. Liu, "Electrically pumped continuous-wave 1.3-mu m InAs/GaAs quantum dot lasers monolithically grown on Si substrates," IET Optoelectron. **8**(2), 20–24 (2014).
18. D. Jung, J. Norman, Y. T. Wan, S. T. Liu, R. Herrick, J. Selvidge, K. Mukherjee, A. C. Gossard, and J. E. Bowers, "Recent Advances in InAs Quantum Dot Lasers Grown on On-Axis (001) Silicon by Molecular Beam Epitaxy," Phys. Status Solidi A **216**(1), 1800602 (2019).
19. A. Y. Liu and J. Bowers, "Photonic Integration With Epitaxial III-V on Silicon," IEEE J. Sel. Top. Quantum Electron. **24**(6), 1–12 (2018).

Optics EXPRESS

20. M. C. Tang, S. M. Chen, J. Wu, Q. Jiang, V. G. Dorogan, M. Benamara, Y. I. Mazur, G. J. Salamo, A. Seeds, and H. Y. Liu, "1.3-mu m InAs/GaAs quantum-dot lasers monolithically grown on Si substrates using InAlAs/GaAs dislocation filter layers," Opt. Express **22**(10), 11528–11535 (2014).
21. A. Lee, Q. Jiang, M. C. Tang, A. Seeds, and H. Y. Liu, "Continuous-wave InAs/GaAs quantum-dot laser diodes monolithically grown on Si substrate with low threshold current densities," Opt. Express **20**(20), 22181–22187 (2012).
22. M. Y. Liao, S. M. Chen, S. G. Huo, S. Chen, J. Wu, M. C. Tang, K. Kennedy, W. Li, S. Kumar, M. Martin, T. Baron, C. Y. Jin, I. Ross, A. Seeds, and H. Y. Liu, "Monolithically Integrated Electrically Pumped Continuous-Wave III-V Quantum Dot Light Sources on Silicon," IEEE J. Sel. Top. Quantum Electron. **23**(6), 1–10 (2017).
23. Y. Wang, S. M. Chen, Y. Yu, L. D. Zhou, L. Liu, C. C. Yang, M. Y. Liao, M. C. Tang, Z. Z. Liu, J. Wu, W. Li, I. Ross, A. J. Seeds, H. Y. Liu, and S. Y. Yu, "Monolithic quantum-dot distributed feedback laser array on silicon," Optica **5**(5), 528–533 (2018).
24. J. Norman, M. J. Kennedy, J. Selvidge, Q. Li, Y. T. Wan, A. Y. Liu, P. G. Callahan, M. P. Echlin, T. M. Pollock, K. M. Lau, A. C. Gossard, and J. E. Bowers, "Electrically pumped continuous wave quantum dot lasers epitaxially grown on patterned, on-axis (001) Si," Opt. Express **25**(4), 3927–3934 (2017).
25. Y. T. Wan, J. Norman, Q. Li, M. J. Kennedy, D. Liang, C. Zhang, D. N. Huang, Z. Y. Zhang, A. Y. Liu, A. Torres, D. Jung, A. C. Gossard, E. L. Hu, K. M. Lau, and J. E. Bowers, "1.3 mu m submilliamp threshold quantum dot micro-lasers on Si," Optica **4**(8), 940–944 (2017).
26. Y. T. Wan, D. Jung, J. Norman, C. Shang, I. MacFarlane, Q. Li, M. J. Kennedy, A. C. Gossard, K. M. Lau, and J. E. Bowers, "O-band electrically injected quantum dot micro-ring lasers on on-axis (001) GaP/Si and V-groove Si," Opt. Express **25**(22), 26853–26860 (2017).
27. Q. Li, Y. T. Wan, A. Y. Liu, A. C. Gossard, J. E. Bowers, E. L. Hu, and K. M. Lau, "1.3-mu m InAs quantum-dot micro-disk lasers on V-groove patterned and unpatterned (001) silicon," Opt. Express **24**(18), 21038–21045 (2016).
28. W. Q. Wei, J. Y. Zhang, J. H. Wang, H. Cong, J. J. Guo, Z. H. Wang, H. X. Xu, T. Wang, and J. J. Zhang, "Phosphorus-free 1.5 mu m InAs quantum-dot microdisk lasers on metamorphic nGaAs/SOI platform," Opt. Lett. **45**(7), 2042–2045 (2020).
29. M. Bruel, B. Aspar, and A. J. AubertonHerve, "Smart-cut: A new silicon on insulator material technology based on hydrogen implantation and wafer bonding," Jpn. J. Appl. Phys. **36**(Part 1, No. 3B), 1636–1641 (1997).
30. A. Tauzin, T. Akatsu, M. Rabarot, J. Dechamp, M. Zussy, H. Moriceau, J. E. Michaud, A. M. Charvet, L. Di Cioccio, F. Fournel, J. Garrione, B. Faure, F. Letertre, and N. Kernevez, "Transfers of 2-inch GaN films onto sapphire substrates using Smart Cut (TM) technology," Electron. Lett. **41**(11), 668–670 (2005).
31. M. Webb, C. Jeynes, R. Gwilliam, P. Too, A. Kozanecki, J. Domagala, A. Royle, and B. Sealy, "The influence of the ion implantation temperature and the dose rate on smart-cut (c) in GaAs," Nucl. Instrum. Methods Phys. Res., Sect. B **240**(1-2), 142–145 (2005).
32. J. J. Lin, T. G. You, M. Wang, K. Huang, S. B. Zhang, Q. Jia, M. Zhou, W. J. Yu, S. Q. Zhou, X. Wang, and X. Ou, "Efficient ion-slicing of InP thin film for Si-based hetero-integration," Nanotechnology **29**(50), 504002 (2018).
33. J. J. Lin, T. G. You, T. T. Jin, H. Liang, W. J. Wan, H. Huang, M. Zhou, F. W. Mu, Y. Q. Yan, K. Huang, X. M. Zhao, J. X. Zhang, S. M. Wang, P. Gao, and X. Ou, "Wafer-scale heterogeneous integration InP on trenched Si with a bubble-free interface," APL Mater. **8**(5), 051110 (2020).
34. Y. Bai, G. D. Cole, M. T. Bulsara, and E. A. Fitzgerald, "Fabrication of GaAs-on-Insulator via Low Temperature Wafer Bonding and Sacrificial Etching of Ge by XeF2," J. Electrochem. Soc. **159**(2), H183–H190 (2011).
35. K. Sumita, J. Takeyasu, K. Toprasertpong, M. Takenaka, and S. Takagi, "Influence of layer transfer and thermal annealing on the properties of InAs-On-Insulator films," J. Appl. Phys. **128**(1), 015705 (2020).
36. N. Hayafuji, S. Ochi, M. Miyashita, M. Tsugami, T. Murotani, and A. Kawagishi, "EFFECTIVENESS OF ALGAAS/GAAS SUPERLATTICES IN REDUCING DISLOCATION DENSITY IN GAAS ON SI," J. Cryst. Growth **93**(1-4), 494–498 (1988).
37. K. Wieteska, W. Wierzchowski, W. Graeff, and G. Gawlik, "X-ray synchrotron diffraction studies of III-V semiconductor compounds implanted with hydrogen," phys. stat. sol. (a) **203**(2), 227–235 (2006).
38. K. Gutjahr, M. Reiche, and U. Gosele, "Contamination and cleaning of GaAs-(100) surfaces," *Icds-18 - Proceedings of the 18th International Conference on Defects in Semiconductors*, Pts 1-4 196, 1967–1971 (1995).
39. P. E. Raynal, M. Rebaud, V. Loup, L. Vallier, M. C. Roure, M. Martin, J. P. Barnes, and P. Besson, "GaAs WET and Siconi Cleaning Sequences for an Efficient Oxide Removal," ECS J. Solid State Sci. Technol. **8**(2), P106–P111 (2019).
40. Y. H. Wang, W. C. Liu, S. A. Liao, K. Y. Cheng, and C. Y. Chang, "ON THE SURFACE-DEFECTS OF MBE-GROWN GAAS-LAYERS," Jpn. J. Appl. Phys. **24**(Part 1, No. 5), 628–629 (1985).